Supervised Transfer Learning for Multi Organs 3D Segmentation With Registration Tools for Metal Artifact Reduction in CT Images

Hanaa M. Al Abboodi [1], Amera W. Al-funjan [2], Najlaa Abd Hamza [3], Alaa H. Abdullah [1], Bashar H. Shami [4]

[1] *College of Engineering, University of Babylon, Babylon, Iraq*
[2] *College of Education for Pure Sciences, University of Babylon, Babylon, Iraq*
[3] *College of Nursing, University of Baghdad, Baghdad, Iraq*
[4] *Biomedical Development Research, Amman, Jordan*

Abstract – **Radiological diagnostics are undeniably crucial in everyday healthcare. CT scans can sometimes provide misleading clues and delay successive treatment due to artifacts caused by reflected radiation from metallic implants. This work successfully segments multiple organs containing metal implants and discards artifacts using a combination of non-rigid transformations, Scribbles-based segmentation, and a pre-trained auto segmentation model (DynaUnet -Pretrained-Model). The presented transfer learning model combined the benefits of an interactive environment and reduced computational and processing-time costs. The transfer learning model proved high auto segmentation performance for multi-organs with metal implants' presence by decreasing metal artefact's impact on the segmentation process and the achieved segmentation accuracies between 0.9998 for the spleen and 0.9829 for the stomach.**

1. Introduction

Radiation therapy is widely used to treat cancer, and it entails exposing the patient to high levels of radiation that kill cancer cells while causing minimal harm to healthy tissue. Radiation debris, however, can compromise the efficacy of a therapy plan for patients with metal implants, such as those used for joint replacements or tooth restorations [1], [2], [3]. 3D medical segmentation requires precisely dividing the image into various areas to recognise the metal device and nearby tissue. This work will study the impact of 3D medical segmentation in eliminating radioactive metal implant artifacts. Accurately identifying the metal implant and surrounding tissue using 3D medical segmentation may minimise radiation artifacts and allow for more precise treatment planning. Accurately placing the metal implant can also help improve the dose calculation accuracy, which is essential in delivering an effective treatment [9], [10]. Three-dimensional medical segmentation also has the benefit of revealing details about the patient's anatomy that can help identify the location of critical structures, such as organs at risk, that reduce the risk of damaging healthy tissue during radiation therapy. The detailed information provided by 3D medical segmentation can also help improve the treatment plan's accuracy by allowing for more precise targeting of the cancer cells [11], [12]. Medical imaging has become an integral component of contemporary medicine. Radiographs, CT scans, MRI scans, and other imaging modalities and ultrasonography are all examples of medical imaging methods.

While these methods are beneficial, they do have some restrictions. The existence of metal devices, which can create artifacts and conflict with the precision of the images, is one of the most significant drawbacks of medical imaging. Metal artifacts can be produced by various variables, such as the type of metal, the size and form of the device, and its direction concerning the imaging plane. This article will examine how 3D medical segmentation can be used to address the issues caused by radiation on metal implants. Image deformation, signal loss, and line artifacts are issues that can arise from metal implant artifacts. Beam stiffening artifacts, visible in CT images as lines or colouring, are caused by metal devices. Medical segmentation is dividing an image into different areas based on its content [7], [8]. 3D medical segmentation is a technique that uses advanced algorithms to segment medical images in three dimensions. This technique effectively separates other tissues and structures in the body, allowing clinicians to analyse the data more accurately [13]. Overcoming metal implant artefacts in medical imaging with the help of 3D medical segmentation has been proven to be a successful strategy. Clinicians can get more trustworthy information by segmenting the images and removing the metal artifacts that can help diagnose and treat various diseases and illnesses, such as cancer, heart disease, and neurological issues. Removing metal device traces and giving doctors more accurate and dependable data are two ways 3D medical segmentation can solve these obstacles. Because of this, doctors will be able to keep an eye on a patient's condition with greater precision and handle them more efficiently. Having metal devices in the body can introduce various artefacts into diagnostic imaging [14], [15]. Streaks, reflections, and other distortions are examples of artifacts that make it challenging to acquire a precise image. Many methods have been presented for decreasing the size of metal artifacts. Iterative reconstruction algorithms are one of these methods presented by [11]. This technique applied iterative methods to reduce artifacts caused by metal implants. It works by simultaneously estimating the image data and the metal location and then updating the estimate iteratively until the artifact is diminished. Dual-energy CT applied two X-ray energies to differentiate between high-attenuating materials like metal and low-attenuating materials like soft tissue to reduce metal artifacts in CT images [12]. Virtual monochromatic imaging applies advanced algorithms to reconstruct images with a single energy level to reduce metal artifacts caused by beam hardening [13]. However, these techniques may not always effectively reduce metal artifacts, especially with large metal implants.

Figure 1 explains CT scan image of an organ with and without the presence of a metal artifact. The organ CT scan image is compared in the presence of metal artifact and not. Where A refers to an organ with a metal implant and its artifact, and B refers to the same original organ image without a metal implant.
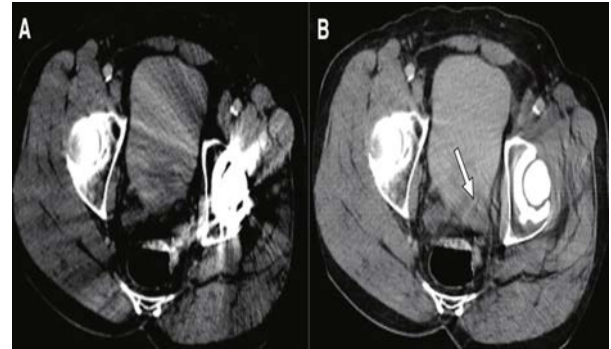

Figure 1.CT scan images of an organ with (image A) and without the presence of a metal artifact (image B).

Artificial intelligence and deep learning techniques are widely recognized as highly advanced methodologies that effectively mitigate the influence of metal artifacts. These techniques involve training computer systems to identify and eliminate artifacts impact by utilizing mathematical procedures in the field of image processing to accurately define these artifacts' features. Many works in literature are found on MAR in radiology images using deep learning and medical image processing algorithms. Most approaches worked in correcting artifacts on a two-dimensional level by applying image processing algorithms to decrease or eliminate artifacts radiation. Recent publications have presented solutions to the challenges in MAR, inspired by the successes of deep learning in handling challenging issues related to MA reduction [17], [18]. The CT image domain metal artifact was reduced by Wang et al. [19], [16] by applying the pix2pix model. U-Net was used by Park et al. [20] to fix sinograms that had been tainted by metal directly. Although these deep learning techniques help diminish metal artifacts, their high expressive power means that neither image nor sinogram domain enhancement can fully restore metal shadows and secondary artifacts meaningless without using deep learning. To improve CT scans, the authors of [1] presented a fully trainable Dual Domain Network (DuDoNet), which trains two convolutional neural networks (CNNs) on dual domains for MA reduction. Researchers in [4] used CGAN deep learning method to generate projections of CT images without the metal artifacts. Then, they reconstructed the original sinogram images by adding the metal implants and subtracting the artifacts labels.

Kyu Song et al. [5] studied the best MAR radiation protocols to decrease metal artifacts for different organ scans and the effect of the dosimetry and projection angles using a phantom model. Also, Nicholas Keat, and Julia F. Barrett [6], studied radiation detection and avoidance protocols for MAR. There were spiral and multi-section method artifacts in the reconstructed images. Some artifacts are reduced by the scanner's software and by design features built into CT scanners. They concluded that the two most essential variables in preventing CT artifacts were cautious patient posture and the optimal selection of scanning settings.

2. Methods and Materials

This study presented various methods to reduce the influence of metal artifacts on the segmentation process in order to achieve an ideal auto segmentation model for multiple organs in the presence of metal implants. These methods included 3D medical segmentation and 3D registration that integrated with supervised learning to achieve this work main objective. The subsequent sections will provide a comprehensive explanation of these methods.

2.1. 3D Medical Segmentation

The process of 3D medical segmentation typically involves several steps. These steps include a pre-processing stage of preparing the medical image for segmentation, which refers to the first step. The pre-processing stage may involve removing noise, enhancing contrast, or adjusting the image intensity. Second, the exact area of the image where the metal implant is may be identified by using the Region of Interest (ROI) tool. This step is typically done manually by a radiologist or medical technician. Third, the segmentation stage involves using algorithms to separate the metal implant from the surrounding tissue. This step can be done using various techniques, including thresholding, region growing, or active contours. Lastly, post-processing involves refining the segmentation results to improve accuracy. It may include the removal of minor artifacts or the filling of image gaps [21].

2.2. 3D Registration

Multiple three-dimensional datasets must be aligned to a standard coordinate system for 3D registration to succeed [22]. Various medical imaging applications require it, including metal artifact reduction (MAR). Metal artefacts may severely degrade CT and MRI images, making precise diagnosis and treatment planning challenging.

By processing raw image data, MAR requires reducing metal artifacts to produce an anatomically accurate patient representation. Using 3D registration techniques to align pre and postoperative patient scans is one approach to MAR. This method utilises the pre-operative scan as a reference and aligns the postoperative scan. Considering the presence of metal artifacts, the registration procedure entails locating the transformation that transfers the postoperative scan onto the pre-operative scan. The aligned postoperative scan can reconstruct an image of the patient's anatomy without artifacts [23]. Multiple 3D registration strategies, such as intensity-based, feature-based, and hybrid approaches, may be used in MAR. Images are aligned using intensity values in intensity-based processes.

On the other hand, image alignment using feature-based strategies relies on unique image characteristics like corners and edges. Hybrid approaches use intensity-based and feature-based techniques to enhance registration precision [24]. Non-rigid registration is a technique that allows for the alignment of images with deformable structures such as the human body. It is a valuable technique for Metal Artifact Reduction (MAR) because metal implants can cause significant distortions in surrounding tissues. Non-rigid registration techniques can account for these distortions and help reduce metal artifacts. Non-rigid segmentation identifies and separates regions of interest in an image with non-linear or deformable boundaries. One common approach to non-rigid segmentation is to use a deformable model, such as a level set or active contour, that evolves to fit the edges of the desired regions. The mathematical equation for a level set deformable model is:

$$\frac{\partial \varphi}{\partial t} + \propto \varphi |(\nabla \varphi)| (k - \delta) = 0 \ldots \ldots \ldots \ldots \ldots (1)$$

Where φ refers to the level set function, t is time, α refers to a parameter that controls the speed of the level set propagation. ψ is a function that penalises the length of the level set curve, $|\nabla \varphi|$ is the magnitude of the gradient of φ, κ is the curvature of the level set curve, and δ is a function that penalises the deviation of φ from a signed distance function [25]. Region growing and thresholding are two image segmentation techniques that can be used with non-rigid registration to reduce metal artifacts. Region growing involves selecting a seed point in the image and iteratively adding neighbouring pixels that meet specific criteria until an entire region is formed.

Thresholding is a straightforward image segmentation method that divides an image into regions depending on the intensity levels of its respective pixels. Thresholding consists in setting a threshold value for pixel intensity and assigning all pixels above that threshold to a particular part. All pixels with intensity values above or below the threshold are labelled foreground or background. The mathematical equation for thresholding is:

$$T(x,y) = 1, if\ I(x,y) > T = 0 \ …..(2)$$

Where T is the threshold value, I(x, y) is the intensity value of the pixel at location (x, y), and T(x, y) is the resulting label of the pixel at location (x, y) [24].

Scribbles-based registration is another approach that involves the user drawing scribbles on the image to indicate the areas that should be aligned. The scribbles guide the registration algorithm, allowing it to focus on the most critical regions for reducing metal artifacts. Growing from seed registration is another technique that involves selecting one or more seed points in the image and adding neighbouring pixels, most like the seed points, until a whole region is formed. This technique can help align images with deformable structures, such as the human body, by focusing on the most critical areas for reducing metal artifacts. Overall, non-rigid registration, region growing, thresholding, scribbles-based, and growing from seed registration are all effective techniques for reducing metal artifacts in medical imaging. Combining these techniques makes it possible to obtain a more accurate representation of the patient's anatomy, even in the presence of metal implants.

Atlasing refers to mapping different images to a standard coordinate system or space. Atlasing has typically been done to facilitate comparisons and analyses across other images, such as in medical imaging or neuroscience [26]. The mathematical equations for atlasing depend on the specific method used to achieve image alignment and registration. Here are a few standard techniques and their associated equations:

1- Affine transformation: Affine transformations involve a combination of translation, rotation, scaling, and shearing operations to align images. The mathematical equation for an affine transformation can be expressed as [27]:

$$T(x) = Ax + b……………………….(3)$$

T(x) is the transformed image coordinate, A is a 3x3 matrix that describes the linear transformation, x is the original image coordinate, and b is a 3x1 vector representing the translation [28].

2- non-rigid registration: non-rigid registration techniques allow for more flexible and deformable transformations of images, which can help align images with complex or non-linear deformations. One common approach to non-rigid registration is to use a deformation field, which describes the displacement of each pixel in the moving image to its corresponding location in the fixed image. The mathematical equation for a deformation field can be expressed as:

$$u(x) = x - \varphi(x) ………………….(4)$$

Where u(x) is the displacement vector at pixel location x, and φ(x) is the deformation field that maps each pixel in the moving image to its corresponding location in the fixed image [29].

3-Intensity-based registration: Intensity-based registration methods aim to align images based on the similarity of their intensity values. One common approach to intensity-based registration uses a cost function that measures the similarity between the intensities of the moving and fixed images. The mathematical equation for a cost function can be expressed as:

$$C = \Sigma[\alpha f(x) - \beta m(T(x))]^2 ………………(5)$$

Where f(x) refers to the fixed image intensity at a specific pixel position, x, m (T(x)) refers to the power of the moving image after applying a transformation T(x). α and β are scaling factors, and Σ is the sum of all pixel locations. These equations provide a basic overview of some mathematical concepts involved in atlasing. However, the specifics of atlasing depend heavily on the application and the algorithms and methods used [30].

2.3. Metal Artifact Reduction (MAR) Using Supervised Learning

Supervised learning techniques, such as deep learning, have shown promising results for metal artifact reduction (MAR) in medical imaging. These techniques involve training a model using labelled data to learn the relationship between input images and their corresponding artifact-free images. 3D segmentation is often used in supervised learning for MAR to identify and segment image areas containing metal artifacts. Several registration tools can be used with 3D segmentation for supervised learning in MAR. 3D slicer is a comprehensive software platform for medical image analysis that includes image registration, segmentation, and visualisation tools.

It also provides a user-friendly interface for training and testing deep learning models. The accuracy of deep learning models for MAR may be improved by using these registration techniques with 3D segmentation capabilities to pre-process the medical images for supervised learning.

Regarding medical image annotation and deep learning, MONAI Label is the get-it-to open-source platform [31]. It offers a straightforward method for medical image annotation and creating deep learning model training data. In addition, it has transfer learning-ready models that have already been trained. DynaUNet is a pre-trained deep-learning model that relies on the U-Net architecture applied to perform image segmentation in medical applications. This model is trained using a substantial medical images dataset and can be fine-tuned on a smaller dataset for a specific segmentation task. Researchers may reuse a learned model for a new study using the transfer learning approach, which entails training on a smaller dataset.

MONAI Label and DynaUNet can apply a transfer learning strategy to analyse medical images. For example, it was annotating an entirely new set of medical images using MONAI Label and then using DynaUNet as a basis for training a novel segmentation model. When introducing a new model, transfer learning can lessen the amount of labelled data needed and boost the model's performance on the new dataset [5].

2.3.1. Active Learning Strategies with Transfer Learning

In MONAI Label, scribbles are an example of free-form line drawing used for low-intensity interactions between scribble-based models. The first model uses scribbles as a method of producing segmentation labels [31], [6]. Labels inferred by a deep learning model may be improved using scribbles-based refinement model as can be seen in Figure 2.
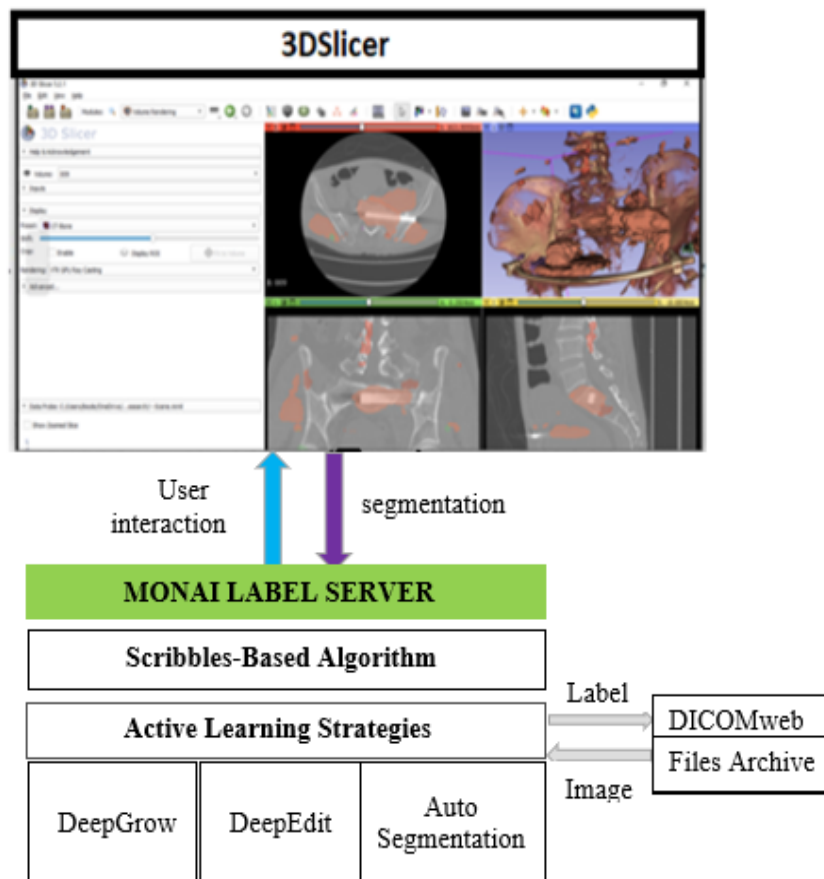

Figure 2. Block diagram of our transfer learning method with MONAI label

Figure 3 explains our complete 3D segmentation, gathering different algorithms using 3DSlicer, MONAI Label, auto segmentation for multi organs, atlasing and thresholding for Metal, Full organs 3D shapes segmented with non-rigid registration of grow from seed and atlasing through active learning. Figure 4 shows the refinement of the complete segmentation organ (stomach here) specific segmentation with scribbles and transfer learning.
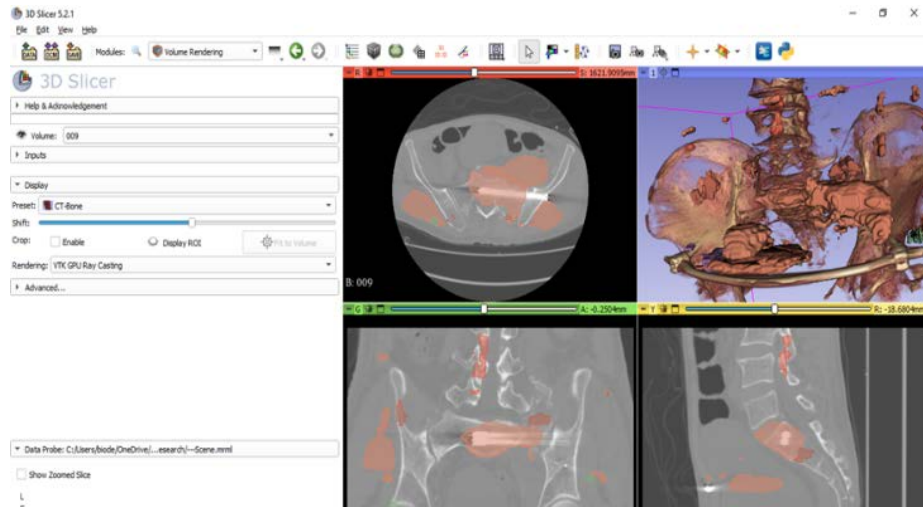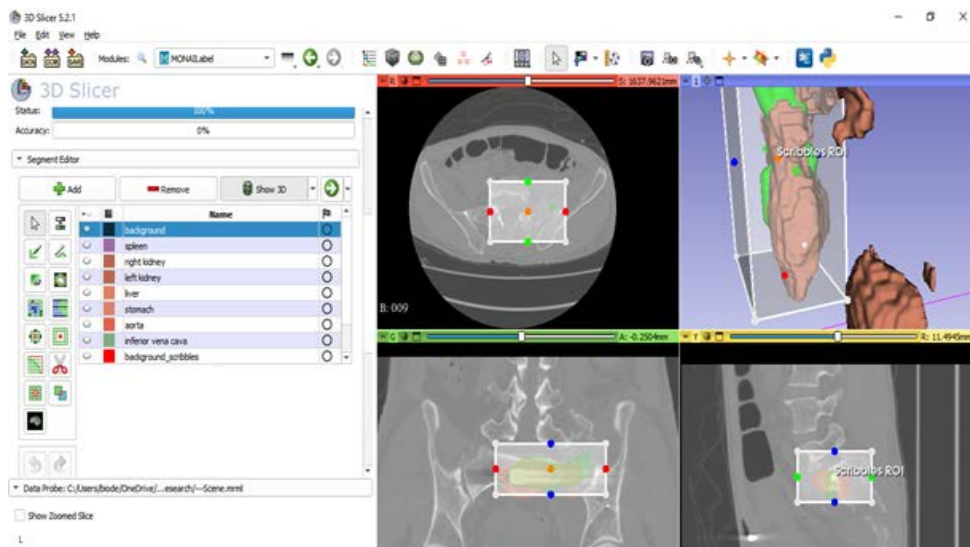

Figure 3. Full 3D segmentation

Figure 4. Refinement of complete segmentation of
stomach organ with scribbles and transfer learning

DynUnet is a deep-learning model architecture that can be trained for various image-processing tasks, such as segmentation, registration, and reconstruction. The mathematical equations for DynUnet would depend on the specific implementation details and training data used. However, the basic architecture of DynaUnet involves convolutional neural networks (CNNs) and recurrent neural networks (RNNs) to perform spatial and temporal processing of image data. The mathematical equations for the CNN and RNN components of DynUnet are as follows [9]:

$$CNN: y = f(Wx + b) \text{...........................(6)}$$

Where x is the input image data, W and b are the weight and bias matrices of the CNN, and f is a non-linear activation function [32], [33].

$$RNN: h_t = g(W_i \cdot h_{t-1} + W_i \cdot x_t + b)\text{........(7)}$$

Where h_t is the hidden state at time t, W_i .h and W_i .x are the weight matrices of the RNN, b is the bias vector, and g is a non-linear activation function [33], [34].

In this work, MONAI Label and DynaUNet have been applied as a transfer learning strategy to analyse our MAR medical images dataset.

The process involved annotating an entirely new set of medical images using MONAI Label and then using DynaUNet as a basis for training a novel segmentation model. When introducing a new model, transfer learning can lessen the amount of labelled data needed and boost the model's performance on the new dataset. Transfer learning segmentation outcomes compared with TotalSegmentator reference pre-trained segmentation model.

The segmentation performs using the transfer Learning segmentation method based on the annotated ROI. Similarly, the TotalSegmentator pre-trained model was used to perform segmentation on the same ROI. Both segmentations have been exported in a DICOM standard format.

2.3.2. *Model Configuration and MAR Dataset*

The 104 whole-body structures in the TotalSegmentator datasets serve as the training set [35]. Large volumes of structures in CT scans are a problem for TotalSegmentator. Voxel-wise multi-label segmentation is used to divide up 104 different types of tissue. The gradient descent approach improves the model by minimising the Dice cross-entropy loss between the model's predicted mask and the ground truth segmentation. The 32 GB of GPU memory was used for the training. The actual input to the model is 96 by 96 by 96. The learning rate is 1e-4, and Adam is the optimiser. Label 0 was selected as the background category (everything else), while labels 1-105 were selected as foreground classes (105) in a CT picture where the loss function was a dice loss. The gradient descent approach improves the model by reducing the difference in dice cross-entropy between the trained model's predicted mask and the ground-truth segmentation.

Before using the bundle, it needs to download the data and combine all the annotated labels into a single NIFTI file. The bundle with MONAI Label has been placed to the test with latencies and memory performance using an image with dimensions of (512, 512, 397) and a slice thickness of 1.5mm. After being down-sampled to an isotropic resolution of 1.5, the size of the image being evaluated is now (287, 287, 397). 1.5 mm model (Single Model with 104 foreground classes) performs well with 28.73G of GPU and 26G of CPU. The dataset for MAR used to run our transfer learning model for organ auto segmentation is a 3d CT dataset of bones and metal implants within. A dataset for pelvic bone CT with implants has been chosen to preform our model for multi organs auto segmentation in the presence of metal artifact. Before their work in 3D segmentation of pelvic bones in various clinical conditions, one of their dataset categories was selected, which is our concern: Pelvic Bones with Metals [36].

3. Results and Discussion

This study introduces a segmentation model employing transfer learning along with supervised learning. The utilization of a transfer learning model demonstrated significant improvements in the performance of auto segmentation for multi-organs in the presence of metal implants. This improvement was achieved by mitigating the negative impact of metal artifacts on the segmentation process. The application of 3D supervised transfer learning and registration techniques has been employed in order to reduce the presence of metal artifacts (MA) in computed tomography, or CT, images. The outcomes of our proposed model have been compared with the TotalSegmentator reference pre-trained segmentation model. The segmentation method employing transfer learning was employed to perform segmentation based on the annotated ROI. Similarly, the TotalSegmentator pre-trained model was used to perform segmentation on the same ROI. Both segmentations have been exported in a DICOM standard format. For results evaluation and after the analysis process is completed, the segment comparison module is evaluated using two metrics such as the Dice coefficient and Harsdorf distance. These two metrics were used to compare the performance of the two segmentation methods. Overall, using the segment comparison module of SlicerRT [37] provides a powerful way to compare two segmentations and evaluate their performance using standard metrics. By combining the capabilities of MONAILabel and SlicerRT, we perform sophisticated analyses and gain insights into the strengths and weaknesses of different segmentation techniques.

To validate our transfer learning model, we compare segmentation results for each organ to validate the model and calculate the validation accuracy of our segmentation in the presence of a metal implant; we refine the tuned transfer learning DynaUnet model.
Figures (5, 6, 7, 8, 9, 10) show segmentation in four stages by transfer learning model for all classes (organs) chosen by DynaUnet pre-trained model auto segmentation, which includes metals thresholding labels (Supervised). These four images are cross-sections of a three-dimensional image obtained at different angles.

First, employ a pre-trained model (transfer learning) for spleen segmentation, which is auto segmentation in the presence of metals, then utilise scribbles for segmentation by active learning until performing another segmentation optimiser that gives more adjustment in the spleen image, and finally compare the two via registration (aligning the segmentation obtained with the original from TotalSegmentator) to ensure that no metal artifacts remain visible.
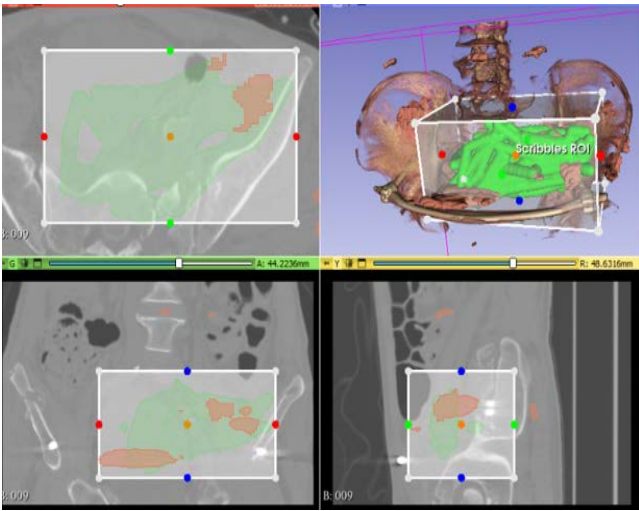
Figure 5. Liver auto segmentation stages in the presence of metals using transfer learning model.
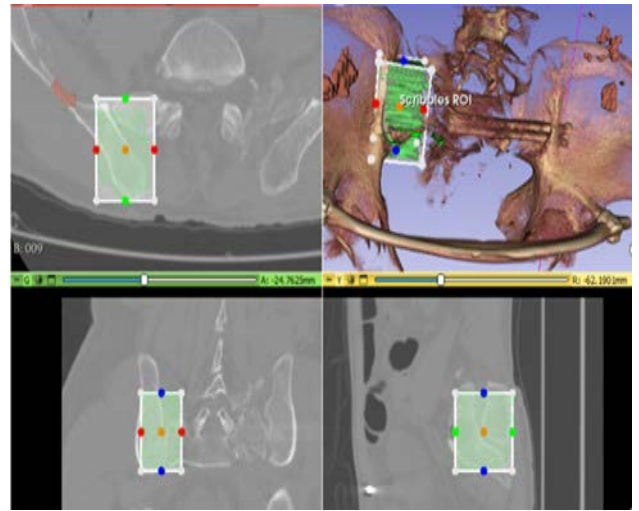

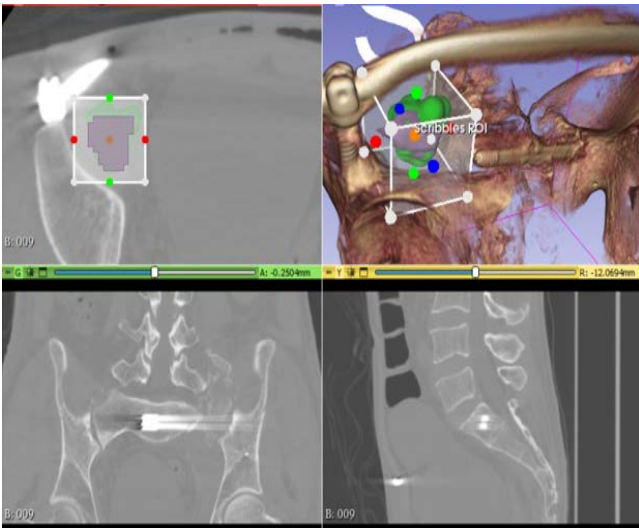*Figure 8. Right kidney auto segmentation stages in the presence of metals using transfer learning model.*

Figure 6. Using a transfer learning model, Spleen auto-segmentation stages in the presen ce of metals.
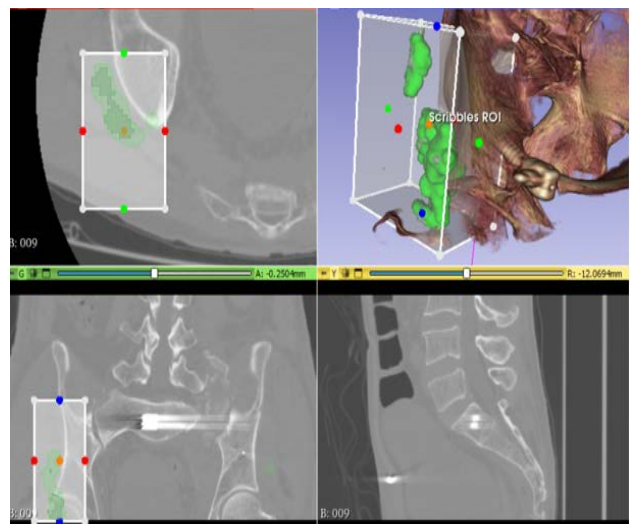

Figure 9. Inferior vena cava auto segmentation stages in the presence of metals using transfer learning model.
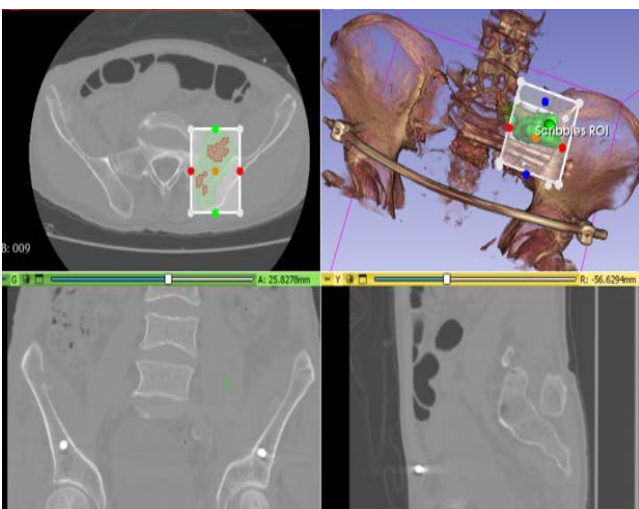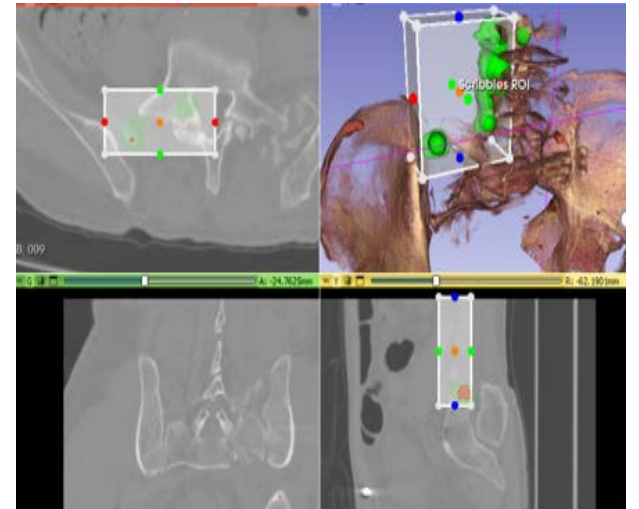

Figure 7. Left kidney auto segmentation stages in the presence of metals using transfer learning model.

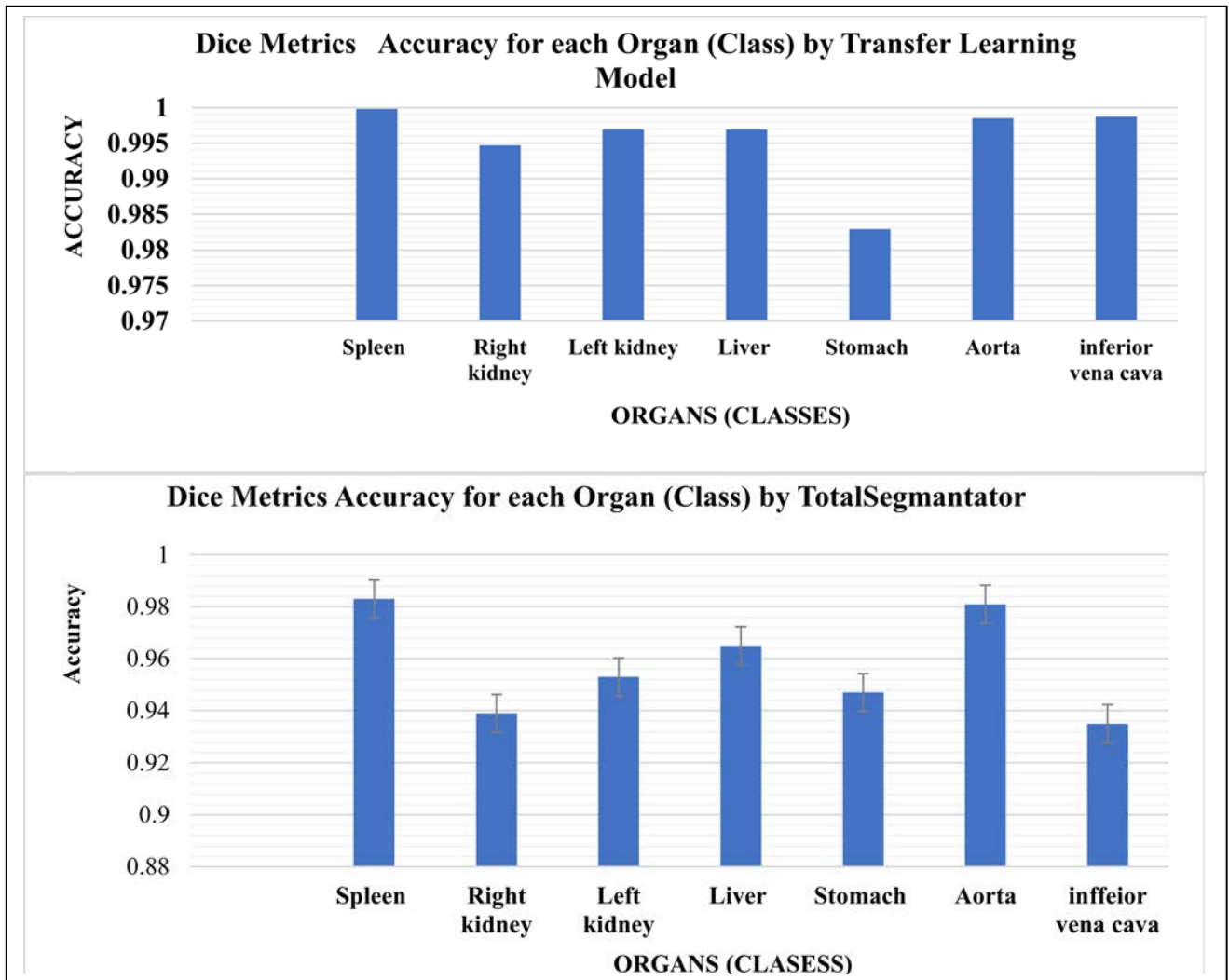*Figure 10. Aorta auto segmentation stages in the presence of metals using transfer learning model.*

Figure 11. Performances comparison between auto segmentation for all classes (organs) with metal implant participated in our transfer learning model with Totalsegmentator original model and its data without a metal implant.

Based on Table 1 experimental results, the accuracy range achieved by applying the transfer learning model was from 0.98 to 0.999, including the organ image reconstruction accuracy for seven organs involved in our work.

It reached a dice score of 0.9985 for the aorta segmentation. The organs that participated in this work are the inferior vena cava, aorta, spleen, liver, stomach, and right and left kidneys. Harsdorff similarity distance was computed to evaluate our model performance in accurate organ segmentation despite the metal artifact's presence, as shown in Table 2. The dice value for the inferior vena cava was 0.9987, making the Harsdorff similarity distance 70.836. The left kidney had a dice score of 0.9969 and a Harsdorff similarity distance of 99.8976.

Harsdorff similarity distance for the liver decreased to 40.8221 despite a dice score of 0.9969. The Harsdorf for the right kidney is 58,902 (0,9947 on the dice). Harsdorff of 95.7455 for spleen when the score was 0.9998 and finally dice score of 0.9829 for stomach with Harsdorff of 37.9819. These analytical findings demonstrate a high segmentation score even in the presence of a metal implant. However, the experimental results proved that a metal implant's presence did not affect the correctness segmentation even if the organ was positioned in the field of view of the metal implant. Figure 11 explains the performances comparison between auto segmentation for all classes (organs) with metal implant participated in our transfer learning model with Totalsegmentator original model and its data without a metal implant.

Table 1. Results of dice metrics scores for our transfer learning model for all selected classes (organs) compared with Totalsegmentator original model and the reference segment is foreground scribbles.

Metric name	Metric value						
Compare segment	aorta	inferior vena cava	left kidney	liver	right kidney	spleen	stomach
Dice coefficient	0.30286	0.464946	0.189151	0.227128	0.0392095	0.699201	0.206863
True positives (%)	0.0325581	0.057477	0.0361229	0.2898	0.0108554	0.026915	0.223631
True negatives (%)	99.8176	99.8102	99.6542	97.7379	99.4571	99.9499	98.0615
False positives (%)	0.0156123	0.00921447	0.10239	1.09762	0.0317376	0.00983764	0.0508961
False negatives (%)	0.134276	0.123073	0.207311	0.874651	0.500266	0.0133202	1.66396
Reference center	(29.8378, -1.13531, 1686.48)	(109.932, -14.6382, 1577.02)	(-33.2131, -13.2093, 1641.6)	(-16.8609, 29.6008, 1603.03)	(68.1684, -30.0134, 1620.01)	(85.0987, 48.3864, 1577.93)	(5.7419, 11.3902, 1612.16)
Compare center	(29.2333, -3.3537, 1654.61)	(88.6246, -16.7035, 1581.48)	(-6.96035, -21.6994, 1620.32)	(37.3081, 0.0095101, 1605.45)	(39.9987, -3.47126, 1629.68)	(81.9266, 40.222, 1584.68)	(-9.28752, -0.250403, 1622.49)
Reference volume (cc)	29.3209	31.7316	42.7833	204.651	89.8292	7.0713	111.589
Compare volume (cc)	8.46591	11.721	24.3435	243.838	7.4857	6.45925	16.2293
Accuracy	0.9985	0.9987	0.9969	0.9969	0.9947	0.9998	0.9829

Table 2. Results of Harsdorf 3D similarity distance scores for our transfer learning model for all chosen classes (organs) compared with Totalsegmentator original model and the reference segment is foreground.

Metric name	Metric value						
Compare segment	**aorta**	**inferior vena cava**	**left kidney**	**liver**	**right kidney**	**spleen**	**stomach**
Maximum (mm)	148.077	196.353	132.431	119.377	166.056	122.635	79.4385
Average (mm)	21.7632	15.8941	15.2395	25.9705	41.6591	9.81264	15.605
95% (mm)	70.836	99.8976	40.8221	58.9002	95.7455	47.4621	37.9819

4. Conclusion

Based on the research on the advantages of 3D supervised transfer learning and registration techniques to eliminate metal artifacts (MA) in CT images, it can be concluded that these techniques significantly improve the clarity of medical images in the presence of metal. The use of pre-trained models and auto-segmentation techniques reduces the impact of metal artifacts on the segmentation accuracy of the spleen member, for instance, and scribble segmentation with active learning further refines the segmentation process. The registration process ensures that the obtained segmentation aligns with the original from TotalSegmentator, allowing for accurate and precise visualisation of the spleen. These techniques eliminate the harmful effects of metal artifacts on image quality and provide a reliable solution for medical imaging applications. This research demonstrates the efficacy of active transfer learning for improving the accuracy of medical image segmentation and the potential benefits of 3D supervised transfer learning and registration techniques in other medical imaging applications. Future works can be as follows: Integration of deep learning techniques: As deep learning algorithms continue to advance, integrating them into the current 3D supervised transfer learning and registration techniques could potentially improve the accuracy and efficiency of the segmentation process. Exploration of other registration techniques: This study used registration to align the obtained segmentation with the original from TotalSegmentator. However, exploring other registration techniques could lead to even more accurate results. Clinical validation: Future studies could validate the effectiveness of these techniques in a clinical setting to assess their impact on patient outcomes, diagnostic accuracy, and treatment planning. The generalisation to other imaging modalities: Although this study focused on CT images, it would be interesting to explore the generalizability of these techniques to other imaging modalities, such as MRI or PET, where metal artifacts can also impact image quality.

References:

[1]. Lin, W. A., Liao, H., Peng, C., Sun, X., Zhang, J., Luo, J.,& Zhou, S. K. (2019). Dudonet: Dual-domain network for ct metal artifact reduction. In *Proceedings of the IEEE/CVF Conference on Computer Vision and Pattern Recognition*, 10512-10521.

[2]. Zhang, X., Yang, W., Hu, Y., & Liu, J. (2018). DMCNN: Dual-domain multi-scale convolutional neural network for compression artifacts removal. In *2018 25th IEEE international conference on image processing (icip)*, 390-394.

[3]. Guo, J., & Chao, H. (2016). Building dual-domain representations for compression artifacts reduction. In *Computer Vision–ECCV 2016: 14th European Conference, Amsterdam, The Netherlands, October 11–14, 2016, Proceedings, Part I 14*, 628-644. Springer International Publishing.

[4]. Ghani, M. U., & Karl, W. C. (2019). Fast enhanced CT metal artifact reduction using data domain deep learning. *IEEE Transactions on Computational Imaging*, 6, 181-193.

[5]. Song, O. K., Chung, Y. E., Seo, N., Baek, S. E., Choi, J. Y., Park, M. S., & Kim, M. J. (2019). Metal implants influence CT scan parameters leading to increased local radiation exposure: A proposal for correction t echniques. *Plos one*, 14(8), e0221692.

[6]. Barrett, J. F., & Keat, N. (2004). Artifacts in CT: recognition and avoidance. *Radiographics*, 24(6), 1679-1691.

[7]. He, Y., Yang, D., Roth, H., Zhao, C., & Xu, D. (2021). Dints: Differentiable neural network topology search for 3d medical image segmentation. In *Proceedings of the IEEE/CVF Conference on Computer Vision and Pattern Recognition*, 5841-5850.

[8]. Hatamizadeh, A. et al. (2022). Unetr: Transformers for 3d medical image segmentation. In *Proceedings of the IEEE/CVF winter conference on applications of computer vision*, 574-584.

[9]. Ronneberger, O., Fischer, P., & Brox, T. (2015). U-net: Convolutional networks for biomedical image segmentation. *18th International Conference, Munich, Germany, Proceedings, Part III 18*, 234-241. Springer International Publishing.

[10]. Çiçek, Ö., Abdulkadir, A., Lienkamp, S. S., Brox, T., & Ronneberger, O. (2016). 3D U-Net: learning dense volumetric segmentation from sparse annotation. In *Medical Image Computing and Computer-Assisted Intervention–MICCAI 2016: 19th International Conference, Athens, Greece, October 17-21, 2016, Proceedings, Part II 19*, 424-432. Springer International Publishing.

[11]. Herman, G. T., & Lent, A. (1976). Iterative reconstruction algorithms. *Computers in biology and medicine*, 6(4), 273-294.

[12]. Borges, A. P., Antunes, C., & Curvo-Semedo, L. (2023). Pros and Cons of Dual-Energy CT Systems: "One Does Not Fit All". *Tomography*, 9(1), 195-216.

[13]. Pessis, E. et al. (2013). Virtual monochromatic spectral imaging with fast kilovoltage switching: reduction of metal artifacts at CT. *Radiographics*, 33(2), 573-583.

[14]. Zhang, H., Dong, B., & Liu, B. (2018). A reweighted joint spatial-radon domain CT image reconstruction model for metal artifact reduction. *SIAM Journal on Imaging Sciences*, 11(1), 707-733.

[15]. Zhang, Y., & Yu, H. (2018). Convolutional neural network based metal artifact reduction in x-ray computed tomography. *IEEE transactions on medical imaging*, 37(6), 1370-1381.

[16]. Wang, X. et al. (2018). Esrgan: Enhanced super-resolution generative adversarial networks. In *Proceedings of the European conference on computer vision (ECCV) workshops*.

[17]. Khalaf, M., & Dhannoon, B. N. (2022). MSRD-Unet: Multiscale Residual Dilated U-Net for Medical Image Segmentation. *Baghdad Science Journal*, *19*(6), 1603-1603.

[18]. Pan, J., Ren, W., Hu, Z., & Yang, M. H. (2018). Learning to deblur images with exemplars. *IEEE transactions on pattern analysis and machine intelligence*, 41(6), 1412-1425.

[19]. Wang, J., Zhao, Y., Noble, J. H., & Dawant, B. M. (2018). Conditional generative adversarial networks for metal artifact reduction in CT images of the ear. *21st International Conference, Granada, Spain, Part I*, 3-11. Springer International Publishing.

[20]. Park, H. S., Chung, Y. E., Lee, S. M., Kim, H. P., & Seo, J. K. (2017). Sinogram-consistency learning in CT for metal artifact reduction. *arXiv preprint arXiv:1708.00607*, *1*.

[21]. Antonelli, M. et al. (2022). The medical segmentation decathlon. *Nature communications, 13(*1), 4128.

[22]. Hamza, N. A., & Abdul-Majeed, G. H. (2020). A new approach for 3D face modeling using multi-view-stereo and ICP algorithms. *Periodicals of Engineering and Natural Sciences*, 8(2), 960-270.

[23]. Chen, X. et al. (2021). A deep learning-based auto-segmentation system for organs-at-risk on whole-body computed tomography images for radiation therapy. *Radiotherapy and Oncology*, *160*, 175-184.

[24]. Maintz, J. A., & Viergever, M. A. (1996). An overview of medical image registration methods. In *Symposium of the Belgian hospital physicist's association (SBPH/BVZF)*, *12*(5), 1-22.

[25]. Rueckert, D., Sonoda, L. I., Hayes, C., Hill, D. L., Leach, M. O., & Hawkes, D. J. (1999). Non-rigid registration using free-form deformations: application to breast MR images. *IEEE transactions on medical imaging*, *18*(8), 712-721.

[26]. Toga, A. W., & Thompson, P. M. (2001). The role of image registration in brain mapping. *Image and vision computing, 19*, 3-24.

[27]. Umeyama, S. (1991). Least-squares estimation of transformation parameters between two-point patterns. *IEEE Transactions on Pattern Analysis & Machine Intelligence*, *13*(4), 376-380.

[28]. Maintz, J. A., & Viergever, M. A. (1998). A survey of medical image registration. *Medical image analysis*, *2*(1), 1-36.

[29]. Pluim, J. P., Maintz, J. A., & Viergever, M. A. (2003). Mutual-information-based registration of medical images: a survey. *IEEE transactions on medical imaging*, *22*(8), 986-1004.

[30]. Krizhevsky, A., Sutskever, I., & Hinton, G. E. (2017). Imagenet classification with deep convolutional neural networks. *Communications of the ACM*, *60*(6), 84-90.

[31]. Diaz-Pinto, A. et al. (2022). Monai label: A framework for ai-assisted interactive labeling of 3d medical images. *arXiv preprint arXiv:2203.12362*.

[32]. Simonyan, K., & Zisserman, A. (2014). Very deep convolutional networks for large-scale image recognition. *arXiv preprint arXiv:1409.1556.*

[33]. Huang, Z., Xu, W., & Yu, K. (2015). Bidirectional LSTM-CRF models for sequence tagging. *arXiv preprint arXiv:1508.01991.*

[34]. Hochreiter, S., & Schmidhuber, J. (1997). Long short-term memory. *Neural computation*, *9*(8), 1735-1780.

[35]. Wasserthal, J., Meyer, M., Breit, H. C., Cyriac, J., Yang, S., & Segeroth, M. (2022). TotalSegmentator: robust segmentation of 104 anatomical structures in CT images. *arXiv preprint arXiv:2208.05868*.

[36]. Liu, P., Han, H., Du, Y., Zhu, H., Li, Y., Gu, F., ... & Zhou, S. K. (2021). Deep learning to segment pelvic bones: large-scale CT datasets and baseline models. *International Journal of Computer Assisted Radiology and Surgery*, *16*, 749-756.

[37]. Pinter, C., Lasso, A., Wang, A., Jaffray, D., & Fichtinger, G. (2012). SlicerRT: radiation therapy research toolkit for 3D Slicer. *Medical physics*, *39*(10), 6332-6338.